Cellular/Molecular

Amplitude and Kinetics of Action Potential-Evoked Ca^{2+} Current and Its Efficacy in Triggering Transmitter Release at the Developing Calyx of Held Synapse

Yi-Mei Yang and Lu-Yang Wang

The Program for Brain and Behavioral Research and Division of Neurology, The Hospital for Sick Children, and Department of Physiology, University of Toronto, Toronto, Ontario, Canada M5G 1X8

Action potentials (APs) play a crucial role in evoking Ca^{2+} currents (I_{Ca}) through voltage-gated calcium channels (VGCCs) and transmitter release. During development and neuromodulation, both depolarization and repolarization phases of APs change, but how such changes affect the characteristics of I_{Ca} and its efficacy at central synapses is not clear. By paired voltage-clamp recordings of I_{Ca} and excitatory postsynaptic currents (I_{EPSC}) with pseudo-APs and real APs, we examined these issues in the developing calyx of Held synapse of postnatal mice. We found that speeding the AP depolarization rate primarily reduces the number of activated VGCCs, whereas shortening the AP repolarization phase decreases the number of activated VGCCs and accelerates their kinetics. The I_{Ca}–I_{ESPC} relationships are well predicted by the integral but not the amplitude of I_{Ca}, and exhibit development- and temperature-dependent shifts toward left, indicating an enhancement in downstream Ca^{2+} coupling efficacy. Cross-correlation analyses of I_{Ca} and I_{EPSC} evoked by real APs and pseudo-APs demonstrated that AP shortening in the half-width from 0.4 ms at postnatal day 8 (P8)–P12 to 0.27 ms at P16–P18 decreases I_{Ca} integral by 36%, but increases I_{EPSC} by 72% as a result of developmental upregulation in coupling efficacy. These counteracting actions maintain the release fraction evoked by an AP at ~10% of the maximal quantal output. We suggest that AP narrowing is a critical adaptation for the calyx of Held synapse to control the quantal output per AP and is likely important for the efficient use of the readily releasable pool of synaptic vesicles during high-frequency neurotransmission.

Key words: **calyx of Held synapse; action potential; Ca^{2+} current; transmitter release; developmental plasticity; temporal fidelity**

Introduction

Pioneer work in several invertebrate synapses has demonstrated that the waveform of action potentials (APs) is a crucial element in regulating Ca^{2+} influx into nerve terminals and transmitter release (Klein and Kandel, 1980; Llinas et al., 1981, 1982; Augustine, 1990; Delaney et al., 1991). However, typical central synapses are too small to access, having largely precluded biophysical analysis of voltage-gated Ca^{2+} channels (VGCCs) and their couplings to transmitter release. Recent establishment of optical techniques (Sabatini and Regehr, 1996) and model preparations with large terminals (Forsythe, 1994; Borst et al., 1995; Geiger and Jonas, 2000) has led to the first quantitative description of the interplay between the AP waveform, Ca^{2+} influx, and quantal output in central synapses, but a series of issues arise from such studies. First, contrary to the findings in invertebrate synapses, in which only a small fraction of VGCCs are activated by an AP (Llinas et al., 1982; Augustine, 1990), these studies demonstrate that an AP can effectively open the majority of VGCCs (Sabatini and Regehr, 1997; Borst and Sakmann, 1998, 1999; Geiger and Jonas, 2000; Bischofberger et al., 2002). Second, at squid giant synapse, AP broadening increases the number of activated VGCCs and transmitter release in a linear manner, implying that release of single vesicles can be gated by as few as one channel (Augustine, 1990). In contrast, the fraction of VGCCs activated by an AP at central terminals approaches the submaximum and additional broadening mainly alters the kinetics of VGCCs (Sabatini and Regehr, 1997; Geiger and Jonas, 2000; Bischofberger et al., 2002). Cooperative actions of multiple channels are required for the release of single synaptic vesicles (Wu and Saggau, 1994; Mintz et al., 1995; Borst and Sakmann, 1996; Wu et al., 1999; Fedchyshyn and Wang, 2005). These studies raise the question whether changes in the AP waveform affect the number of activated VGCCs and/or their kinetics selectively or simultaneously. This issue is important not only for understanding different operating modalities for transmitter release among various synapses but also for differentiating subcomponents of Ca^{2+} currents (I_{Ca}) that may be targeted by neuromodulators or pharmacological reagents. Finally, previous studies have been done mostly in immature synapses at room temperature. It is unclear how development and temperature influence I_{Ca} evoked by real APs and consequently the quantal output under physiological conditions.

Received July 17, 2005; revised April 7, 2006; accepted April 17, 2006.

This work was supported by an individual operating grant, "The Synapse" group grant from the Canadian Institutes of Health Research, and by the Burroughs Wellcome Fund (L.-Y.W.). L.-Y.W. holds a Tier II Canada Research Chair. We thank Dr. Milton Charlton for valuable suggestions and other members of the Wang Laboratory for assistance and discussion.

Correspondence should be addressed to Dr. Lu-Yang Wang, Division of Neurology, The Hospital for Sick Children, 555 University Avenue, Toronto, Ontario, Canada M5G 1X8. E-mail: luyang.wang@utoronto.ca.

DOI:10.1523/JNEUROSCI.4889-05.2006

 0270-6474/06/265698-11$15.00/0

In light of these, we have used paired voltage-clamp recordings to investigate the effects of changing AP waveform on I_{Ca} and postsynaptic excitatory currents (I_{EPSC}) at the mouse calyx of Held synapse. We report that the number of VGCCs or their kinetics can each account for approximately one-half of the total Ca^{2+} influx and quantal output. Developmental AP shortening reduces the number of recruited VGCCs and accelerates the kinetics of I_{Ca}, leading to a marked decrease in Ca^{2+} charge transfer at both 22 and 35°C. Quantal output evoked by smaller I_{Ca} is, however, upregulated by a developmental increase in the coupling efficacy.

Materials and Methods

Slice preparation. Mice were housed in the facility certified by the Canadian Council of Animal Care and used for this study according to a protocol approved by the Hospital for Sick Children Animal Care Committee. Brainstem slices were prepared from postnatal day 8 (P8) to P18 mice (CD1×C57 hybrid), similar to that previously described for rats (Forsythe and Barnes-Davies, 1993). After decapitation with a small guillotine, brains were immediately immersed into semifrozen artificial CSF (ACSF) containing the following (in mM): 125 NaCl, 2.5 KCl, 10 glucose, 1.25 NaH_2PO_4, 2 Na-pyruvate, 3 myo-inositol, 0.5 ascorbic acid, 26 $NaHCO_3$, 1 $MgCl_2$, and 2 $CaCl_2$ at a pH of 7.3 when oxygenated (95% O_2 and 5% CO_2) followed by rapid dissection. Transverse slices of the auditory brainstem containing the medial nucleus of the trapezoid body (MNTB) were cut at a thickness of 150–250 μm using a microtome (VT1000S; Leica Microsystems, Ernst-Leitz-Strasse, Wetzler, Germany) followed by incubation at 37°C for 1 h before experimentation. For current-clamp recordings of real APs, thicker slices (250 μm) were used to preserve afferent axons. For paired voltage-clamp recordings, thinner slices (150–200 μm) were prepared to minimize presynaptic axon length and reduce voltage-clamp errors. Most experiments were performed at room temperature (~22°C), except for a subset of experiments in Figure 7, which were performed at 35°C using an inline heater with feedback thermistor (TC-324B; Warner Instruments, Hamden, CT).

Electrophysiology. All recordings were made with a dual-channel amplifier (MultiClamp 700A; Molecular Devices, Union City, CA). ACSF was supplemented with bicuculline (10 μM) and strychnine (1 μM) to block inhibitory inputs during recording. For recording of presynaptic I_{Ca}, tetrodotoxin (0.5 μM), tetraethylammonium (TEA) (10 mM) and 4-aminopyridine (4-AP) (0.3 mM) were added to block Na^+ and K^+ channels respectively, whereas extracellular Ca^{2+} concentration ($[Ca^{2+}]_e$) was set at 1 mM. Patch electrodes were fabricated from thin-wall glass with filaments (World Precision Instruments, Sarasota, FL) and coated with dental wax under a dissection microscope. Resistances of these pipettes were 4–6 MΩ for presynaptic terminals and 2.5–3 MΩ for postsynaptic neurons. For paired voltage-clamp recordings, presynaptic and postsynaptic series resistances were 6–10 MΩ and 4–8 MΩ, respectively, and compensated to 90%. Cells showing higher resistances were omitted from the analysis. Intracellular recording solution for presynaptic I_{Ca} contained the following (in mM): 10 CsCl, 40 HEPES, 0.5 EGTA, 1 $MgCl_2$, 2 ATP, 0.5 GTP, 12 phosphocreatine, 20 TEA, and 3 K-glutamate, and pH adjusted to 7.3 with CsOH. Intracellular solution for postsynaptic recordings contained the following (in mM): 97.5 K-gluconate, 32.5 CsCl, 5 EGTA, 10 HEPES, 1 $MgCl_2$, 30 TEA, and 3 lidocaine *N*-ethyl bromide, pH 7.2. The holding potential was −70 or −80 mV for presynaptic terminals and −60 mV for postsynaptic neurons, respectively. Presynaptic I_{Ca} was evoked by various voltage-command paradigms, indicated in the text, and subtraction of capacitive current and leak was done with the on-line P/4 protocol. Real APs were recorded from calyces at a sampling rate of 50 kHz and a filtering frequency of 4 kHz in the current-clamp configuration by stimulating afferent axon fibers with a bipolar platinum electrode. The intracellular solution contained the following (in mM): 97.5 K-gluconate, 32.5 KCl, 0.5 EGTA, 40 HEPES, and 1 $MgCl_2$, pH 7.3 (no supplement of glutamate). After manually removing stimulation artifacts preceding the APs, the digitized values were used as voltage-command templates and fed back into the amplifier as stimulation files (Axon Text File) through pCLAMP 8 software at the same frequency as their acquisition (50 kHz). These real APs were then used as presynaptic voltage-command waveforms for experiments in Figures 1, 6, and 7. Details for pseudo-APs and real APs as voltage-clamp paradigms are given in the text and figure legends. Reagents were from Sigma (St. Louis, MO), Tocris Bioscience (Ellisville, MO), and Alomone Labs (Jerusalem, Israel).

Voltage-clamp quality and stability of I_{Ca} and I_{EPSC} evoked by APs. A series of pseudo-APs and real APs were used as voltage-clamp templates to evoke presynaptic I_{Ca}. The validity of such an approach relies on the assumption that space clamp of the entire terminal is adequate, so that voltage-clamp command templates delivered through a patch electrode do not degrade via the equivalent circuit with the access resistance (R_s) and membrane capacitance (C_m) in the whole-terminal configuration. We performed three sets of experiments to directly evaluate the quality of voltage clamp and stability of I_{Ca} in our study. In the first set of experiments, two electrodes were patched onto the same calyx and the whole-terminal configuration was sequentially established for each pipette. We delivered a real AP template through one electrode in voltage-clamp mode while the other electrode was used to record changes in membrane potential in current-clamp mode. Figure 1*A* shows such a recording in which patch electrodes were positioned on the opposite side of a synapse with a half-circle distance of ~30 μm between two pipettes (diameter of postsynaptic neuron ~20 μm; left panel). We found that the shape and size of recorded APs were very similar to those of the command AP template except for a short delay time (Fig. 1*A*, right panel), as predicted by the equivalent circuit (i.e., $\tau_D = R_s C_m$). In three such recordings, we estimated the mean τ_D to be 0.18 ± 0.01 ms, whereas the mean amplitude of the recorded AP was decreased by 5.90 ± 2.22 mV or 5.4 ± 2.0% compared with the command template ($n = 3$). These results demonstrated that the fidelity of the AP waveform was largely preserved under our experimental conditions. Although the drop in the AP amplitude may be smaller than 6 mV for membrane area <30 μm away from the patch electrode, it should be noted that even a small decrease in the AP amplitude may have a significant impact on I_{EPSC} (Wu et al., 2004), because I_{EPSC} is a power function of I_{Ca}. To reduce such space-clamp errors and mimic the manner by which axonal APs propagate into the calyx, we positioned the presynaptic patch pipette onto the calyx membrane immediately next to the axon heminode for a majority of experiments included in this study. We found such a technical maneuver was critical for us to maintain low access resistance throughout the experiments (<10 MΩ) and obtain large and fast I_{Ca}. This is particularly important for recordings from P16–P18 calyces that have undergone morphological transformation into thin finger digits, from which delivery of voltage-clamp paradigms to the entire calyx with fidelity is difficult to achieve.

In the second set of experiments, we examined the kinetic changes of I_{Ca} evoked by a real AP in response to elevated extracellular Ca^{2+} concentration. If the quality of voltage clamp was poor, one could predict that significant slowing of activation and deactivation kinetics occur as I_{Ca} grows in size with an increased driving force. Figure 1*B* (left panel) shows the recordings of I_{Ca} in extracellular solutions containing low $[Ca^{2+}]_e$/high $[Mg^{2+}]_e$ (0.5/4.5 mM) and a high $[Ca^{2+}]_e$/low $[Mg^{2+}]_e$ (4/1 mM) ACSF. When *Rs* was kept <10 MΩ, we found that at low and high Ca^{2+} concentrations, the rise times of I_{Ca} were 0.19 ± 0.01 and 0.23 ± 0.03 ms, and decay times were 0.37 ± 0.02 and 0.35 ± 0.03 ms, respectively (Fig. 1*B*, right top panels), which are comparable with those obtained with double-electrode voltage-clamp experiments (Borst and Sakmann, 1998). The kinetics of I_{Ca} was not significantly changed ($p > 0.05$; $n = 4$) despite a nearly fourfold increase (from 0.71 ± 0.17 to 2.61 ± 0.68 nA) in the amplitude of I_{Ca} (Fig. 1*B*, right bottom panel), indicating that voltage-clamp errors are minor. To minimize such errors, all of the subsequent experiments in this study were done in 1 mM $[Ca^{2+}]_e$, which typically allowed generation of I_{Ca} under 2 nA. Low $[Ca^{2+}]_e$ also helped reduce saturation and desensitization of postsynaptic AMPARs.

In the third set of experiments, we examined the stability of I_{Ca} and I_{EPSC} evoked by voltage-clamp AP template after the breakthrough of the presynaptic and postsynaptic patches. We found that under the condition of low $[Ca^{2+}]_e$ (1 mM) and low *Rs* (<10 MΩ), both currents were reasonably stable (Fig. 1*C*, left panels). Compared with the first re-

sponses, I_{Ca} and I_{EPSC} after 10 min of recordings were 93.41 ± 4.29% and 96.08 ± 6.26% ($n = 4$), respectively (Fig. 1*C*, right panels), running down by ~5%. Given this observation, we collected the majority of data within the first 10 min while the sequence of stimulation paradigms for different synapses was randomized so as to reduce the errors attributable to the rundown.

Data analysis. Data were acquired on-line, filtered at 4 kHz, digitized at 50 kHz and analyzed off-line using the pCLAMP 8 software package (Molecular Devices) and Excel 2000 (Microsoft, Redmond, WA). For analyses of the input (I_{Ca})–output (I_{EPSC}) relationship, the I_{Ca} integral was measured using the analysis window that began at the onset of I_{Ca} and ended at the point where the decay phase of I_{Ca} intercepted with baseline; the I_{EPSC} integral was measured from the onset of EPSC to the point at which EPSC decayed back to 10% of the EPSC peak amplitude. Absolute or normalized current integrals were plotted against each other and fitted with the Hill function in the following form: $I_{EPSC} = I_{EPSC\text{-}Max}/[1 + (I_{Ca}/I_{EC50})^{nH}]$, where n_H and I_{EC50} denote the Hill coefficient and the I_{Ca} integral at which the half-maximal I_{EPSC} ($I_{EPSC\text{-}Max}$) was evoked. In some cases, the integral of I_{EPSC} was plotted against the amplitude of I_{Ca} to illustrate their relationship under different experimental conditions (e.g., Fig. 6). All raw traces shown in this study were single sweeps except for I_{Ca} and I_{ESPC} evoked by real APs, which were averages of three sweeps (see Figs. 6, 7). For other correlation analyses, least-squares linear regression was performed using Excel 2000 (Microsoft). Statistical tests of significance were two-tailed, unpaired Student's *t* tests with a *p* value cutoff of <0.05. Data were expressed as the mean ± SE from a population of synapses (*n*).

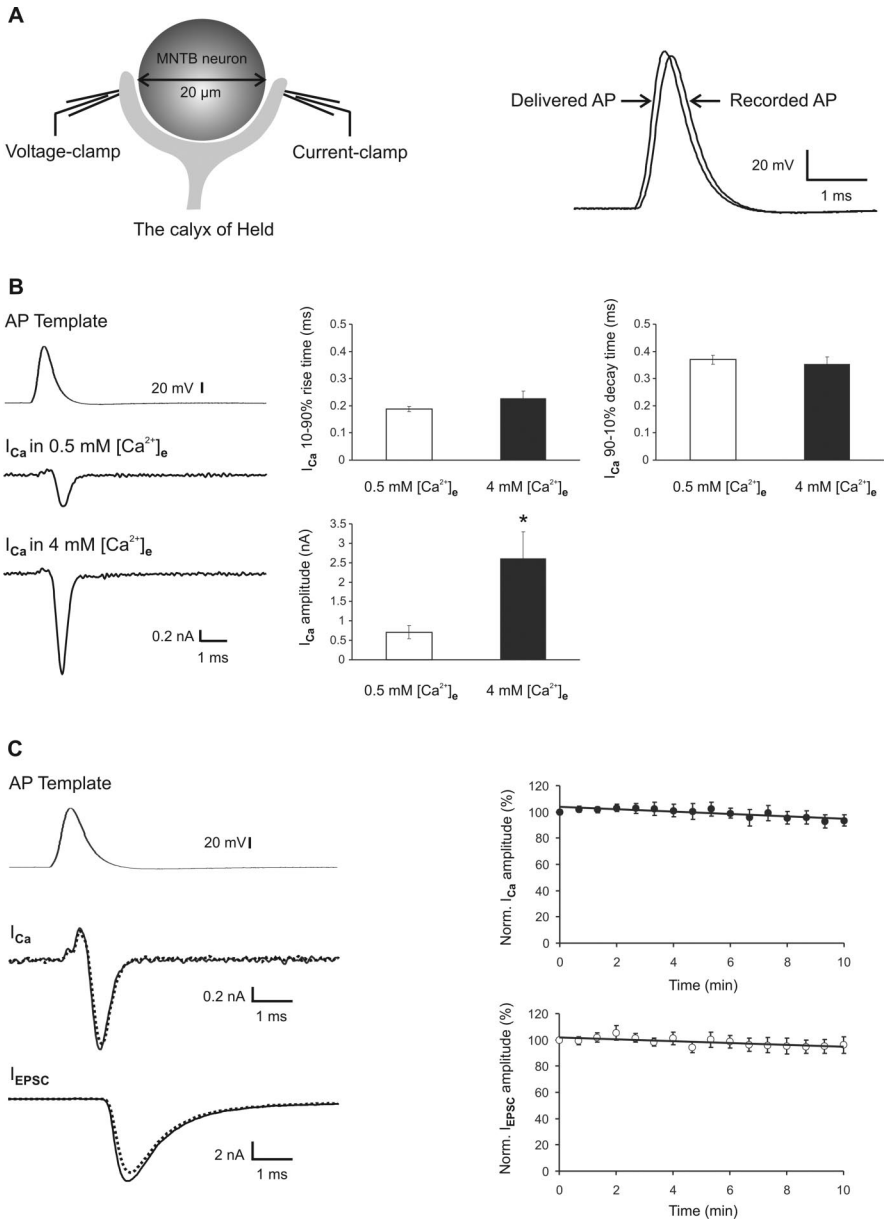

Figure 1. Voltage-clamp quality and stability of presynaptic I_{Ca} and I_{EPSC} evoked by the AP template. ***A***, A diagram showing dual-electrode patch-clamp recordings from the same calyceal terminal enclosing a postsynaptic neuron (diameter ~20 μm) (left panel). The AP template (amplitude, 110 mV, from −70 mV to +40 mV; half-width, 0.6 ms) delivered by an electrode in voltage-clamp mode is superimposed with the recorded AP (right panel) with another electrode in current-clamp mode from the same nerve terminal. ***B***, Presynaptic I_{Ca} recorded in 0.5 mM (middle trace) and 4 mM $[Ca^{2+}]_e$ (bottom trace) in response to the same AP as in ***A*** (top trace). In the right panels, the 10–90% rise time, 90–10% decay time, and amplitude of I_{Ca} at these two concentrations are summarized ($n = 4$). ***C***, I_{Ca} (middle trace) and I_{EPSC} (bottom trace) evoked by the same AP as in ***A*** (top trace) at 0 min (continuous lines) and 10 min (dotted lines) after the breakthrough of presynaptic and postsynaptic patches. The amplitudes of I_{Ca} (top right panel) and I_{EPSC} (bottom right panel) normalized to the first responses are summarized ($n = 4$). Norm., Normalized. The asterisk indicates statistical significance ($p < 0.05$ in this and all subsequent figures).

Results

Distinct effects of AP depolarization and repolarization rate on kinetics of presynaptic I_{Ca}

The calyx of Held synapse is an axosomatic synapse in the auditory brainstem, being capable of high-fidelity neurotransmission at extraordinarily high rates (up to 600 Hz) for sound localization (Trussell, 1999; von Gersdorff and Borst, 2002). During the early postnatal developmental stage (P7–P18) at this synapse, the AP width shortens dramatically because of accelerated depolarization and repolarization rates, whereas the AP amplitude remains relatively unchanged (Taschenberger and von Gersdorff, 2000; Fedchyshyn and Wang, 2005). These changes are presumably attributed to the concurrent upregulation of Na^+ and K^+ conductances (Dodson et al., 2003; Elezgarai et al., 2003; Ishikawa et al., 2003; Leao et al., 2005). However, it is not clear how the depolarization or repolarization rate affects the size and kinetics of presynaptic I_{Ca}. To address this question, we made patch-clamp recordings of I_{Ca}, from visually identified calyces, in response to three sets of AP-like voltage-clamp paradigms that were designed to distinguish the effects of changing each AP component (i.e., depolarization or repolarization) on I_{Ca} (Fig. 2*A–C*, top panels). In the first pseudo-AP-like voltage-clamp paradigm (i.e., AP-DEP) (Fig. 2*A*), the depolarization time was increased from 0.1 to 1 ms whereas the amplitude (130 mV, from −70 mV to +60 mV) and repolarization time (0.4 ms) remained constant. We found that presynaptic I_{Ca} evoked by this voltage paradigm gradually increased in amplitude and eventually saturated (the maximal amplitude: 1.79 ± 0.12 nA, $n = 5$) as the depolarization time was prolonged (Fig. 2*A*, middle panel). When the rise and decay time of I_{Ca} were quantified and plotted against the depo-

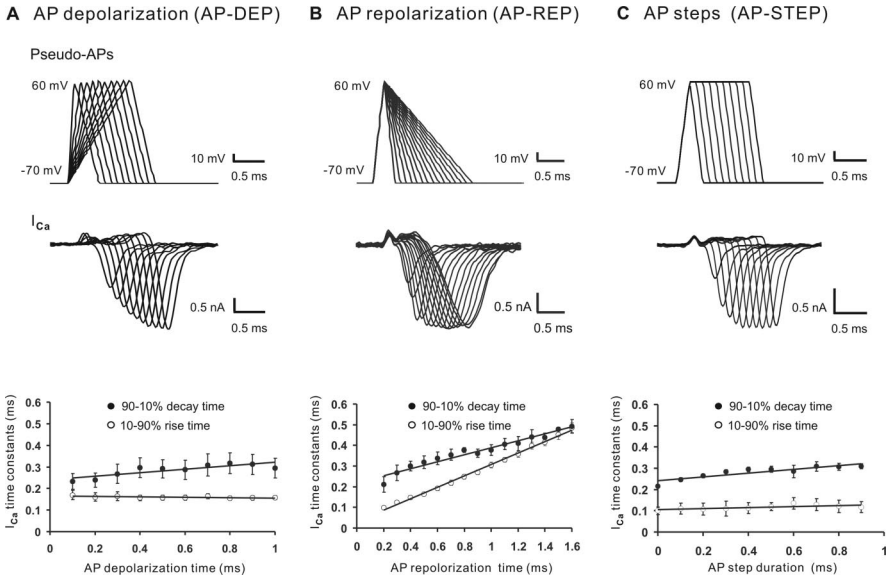

Figure 2. The effects of AP depolarization and repolarization rate on the properties of presynaptic I_{Ca}. ***A–C***, Example recordings of I_{Ca} (middle panels) in response to three sets of AP like voltage ramps (top panels) from −70 to 60 mV: AP-DEP (***A***, depolarization time from 0.1 to 1.0 ms with 0.1 ms increments; repolarization phase, 0.4 ms), AP-REP (***B***, repolarization time from 0.2 to 1.6 ms with 0.1 ms increments; depolarization time, 0.2 ms), and AP-STEP (***C***, plateau duration from 0 to 0.9 ms with 0.1 ms increments; repolarization and depolarization time, 0.2 ms). In the bottom panels, the 10–90% rise time (open circles) and 90–10% decay time (filled circles) of I_{Ca} evoked by these three AP paradigms are summarized. Solid lines are linear regression of the three data sets. All the experiments were done in 1 mM $[Ca^{2+}]_e$ in this and subsequent figures.

larization time, we found that the rise time was ~0.16 ms and unaffected by the changes in the depolarization duration, but the decay time was increased slightly (from 0.23 ± 0.03 to 0.29 ± 0.04 ms, $p > 0.05$; $n = 5$) (Fig. 2*A*, bottom panel). Application of the second voltage paradigm, in which only the repolarization time of pseudo-APs was prolonged (from 0.2 to 1.6 ms) without changing the amplitude and depolarization time (0.2 ms) (i.e., AP-REP) (Fig. 2*B*), initially produced a gradual increase in the I_{Ca} amplitude, which subsequently saturated after the first few pseudo-APs at a level similar (1.49 ± 0.20 nA) to that evoked by AP-DEP paradigm (Fig. 2*B*, middle panel). However, the rise and decay time of I_{Ca} continued to increase (rise time: from 0.10 ± 0.01 to 0.49 ± 0.02 ms, $p < 0.05$; decay time: from 0.21 ± 0.04 to 0.49 ± 0.08 ms, $p < 0.05$; $n = 5$), even after the I_{Ca} amplitude reached its maximum (Fig. 2*B*, bottom panel). Because the driving force for Ca^{2+} in AP-DEP and AP-REP is identical, the similar maximal amplitudes of I_{Ca} generated by the two paradigms likely reflect activity of the same maximal number of recruited VGCCs. However, different kinetic profiles of I_{Ca} in response to AP-DEP and AP-REP raise the possibility that the repolarization phase is not only involved in determining the number of activated VGCCs but also simultaneously affects their kinetics.

To clearly separate the effects of the depolarization and repolarization phase on the number of recruited VGCCs and their kinetics, we designed a third set of pseudo-APs (Fig. 2*C*). In this paradigm, incremental prolongation of plateau duration (0–0.9 ms) was used to recruit an increasing number of VGCCs, while the depolarization and repolarization time course (0.2 and 0.2 ms, respectively) of command voltage ramps were unchanged (i.e., AP-STEP). Because voltage steps to +60 mV in the AP-STEP protocol presumably maximizes the open probability of VGCCs, and the driving force for Ca^{2+} remains constant for all open channels (Borst and Sakmann, 1998, 1999; Gentile and Stanley, 2004; Fedchyshyn and Wang, 2005), the only variable at any given plateau duration would be the number of recruited VGCCs. In response to AP-STEP, we found that I_{Ca} sharply increased in amplitude as the plateau duration was extended (Fig. 2*C*, middle panel) and reached the maximum amplitude of 1.82 ± 0.37 nA within 0.5 ms of plateau duration, but again the rise time was independent of the plateau duration, whereas the decay kinetics showed an increase (from 0.21 ± 0.02 to 0.31 ± 0.03 ms, $p < 0.05$; $n = 5$) (Fig. 2*C*, bottom panel). Under this protocol, the profile of I_{Ca} in its amplitude and kinetics resembled that evoked by AP-DEP (Fig. 2*A*,*C*), except that AP-STEP appeared to be more effective than AP-DEP in evoking I_{Ca}. The increase in the decay time constant of I_{Ca} evoked by AP-DEP and AP-STEP may reflect additional recruitment of distal axonal VGCCs (Borst and Sakmann, 1998) or a different gating mode of calyceal VGCCs in response to prolonged depolarization (e.g., from reluctant to willing mode) (Colecraft et al., 2000).

Together, these three sets of experiments with pseudo-APs suggest that the depolarization and repolarization phases have distinct effects on presynaptic I_{Ca}. The depolarization phase appears to selectively determine the number of recruited VGCCs, whereas the repolarization phase also regulates their kinetics. Hence, subtle changes in AP waveform may potentially provide the nerve terminal with different ways of shaping Ca^{2+} transients. We suggest that the convergent action of shortening both AP depolarization and repolarization phases at the calyx of Held synapse may reduce the amplitude of I_{Ca} and ensure rapid activation and deactivation kinetics of VGCCs and hence fast and brief Ca^{2+} transients. Such changes may be particularly important for controlling the amount of Ca^{2+} influx and transmitter release at this synapse.

Dependence of presynaptic I_{Ca} integral on AP depolarization and repolarization rate

To investigate how depolarization and repolarization rates of an AP influence the amount of Ca^{2+} influx, we quantified the total integral of I_{Ca} evoked by AP-DEP, AP-REP, and AP-STEP. When the first and last sweeps of recorded I_{Ca} in each paradigm were contrasted (Fig. 3*A–C*), it was apparent that the slow kinetics of I_{Ca} evoked by AP-REP led to a significantly greater total integral of I_{Ca} than that generated by AP-DEP or AP-STEP. The maximal I_{Ca} integrals produced by AP-DEP and AP-STEP are comparable (0.66 ± 0.12 nA·ms vs 0.52 ± 0.11 nA·ms, $p > 0.05$) but significantly lower than those evoked by AP-REP (1.18 ± 0.15 nA·ms, $p < 0.05$) (Fig. 3*D*). These results reinforce our interpretation that AP depolarization rate selectively determines the number of activated VGCCs with little effect on their kinetics, whereas AP repolarization rate affects the number and kinetics of recruited channels, both of which contribute to the total Ca^{2+} charge integral during an AP. In Figure 3*E*, I_{Ca} integrals from each of three voltage-clamp paradigms were normalized to their own maximum and plotted against the time of the depolarization, repolarization, or plateau duration. We noted that time-dependent increases in the I_{Ca} integral were well described with a single-exponential function, giving time constants of 0.18, 0.31, and

1.46 ms for AP-STEP, AP-DEP, and AP-REP, respectively. The greater I_{Ca} integral and slower time constants associated with AP-REP imply that the kinetic changes of I_{Ca}, as a result of altering AP repolarization rate, may provide the nerve terminal with a large dynamic range within which the amount of Ca^{2+} inflow during an AP may be fine tuned.

Fractional contribution of the number and kinetics of presynaptic I_{Ca} to quantal output

Knowing that both the number and kinetics of recruited VGCCs by an AP contribute to the total integral of I_{Ca}, we examined the relative contribution of these two components to the maximal quantal output. Using the same synapses, we performed paired recordings in which presynaptic I_{Ca} was evoked with the three sets of voltage-clamp paradigms, whereas I_{EPSC} was simultaneously recorded as readout of transmitter release (Fig. 4). We found that in response to either AP-DEP or AP-STEP, I_{EPSC} grew in size as I_{Ca} increased but remained relatively stable once the amplitude of I_{Ca} reached its maximum (Fig. 4*A*,*C*). However, when the AP-REP paradigm was applied, I_{EPSC} continued to increase even after the amplitude of I_{Ca} had saturated (Fig. 4*B*), implying that the kinetic component of I_{Ca} contributed to the additional Ca^{2+} influx and transmitter release. To quantify these results, we measured the integrals of I_{Ca} and I_{EPSC} and constructed input–output relationships for three pseudo-AP paradigms as shown in Figure 4*D*. We found that the maximal quantal output (I_{EPSC} integral) produced by AP-DEP and AP-STEP was similar (16.40 ± 3.22 nA·ms vs 14.41 ± 2.42 nA·ms, $p > 0.05$, $n = 5$), although these two sets of input–output curves did not overlap. This nonoverlapping profile likely resulted from a difference in the effectiveness of the two protocols in recruiting VGCCs, as illustrated in Figure 3*E*. In contrast, AP-REP activated an increasing number of VGCCs and also prolonged their kinetics, doubling quantal output (28.07 ± 4.26 nA·ms, $p < 0.05$, $n = 5$) compared with AP-DEP and AP-STEP (Fig. 4*D*,*E*). These results suggest that both the number of activated VGCCs and their kinetics are two integral parts of the Ca^{2+} transient evoked by an AP, each of which could contribute up to ~50% of the maximal transmitter release.

By plotting the integral of I_{EPSC} against that of I_{Ca} on a log-log scale, we further examined input–output relationships for three paradigms and found that the slope factors (i.e., calcium cooperativity *m*) derived from linear fits to the data sets generated by AP-DEP and AP-STEP paradigms were very similar (~4) (Fig. 4*F*). However, the input–output relationship for the AP-REP paradigm had two linear components with *m* values being 4.2 and 1.9, respectively. The *m* value for the steep component, which mainly covered data points before the I_{Ca} amplitude became saturated, was similar to those obtained with AP-DEP and AP-STEP paradigms. This is in agreement with our interpretation that the changes in the I_{Ca} amplitude resulting from AP-REP paradigm reflect different numbers of recruited VGCCs, as is also the case for AP-DEP and AP-STEP paradigms. The low *m* value component is likely associated with kinetic changes of I_{Ca}, which become the main contributor to the total I_{Ca} integral after the I_{Ca} amplitude reaches the maximum. Therefore, although the number of recruited channels and their kinetics can each contribute equally to the maximal quantal output, changing the former has much more robust effects on transmitter release than changing the latter. This implies that by changing the depolarization or repolarization time course, nerve terminals may modulate different components underlying the characteristics of the Ca^{2+} transient and cooperative nature of transmitter release.

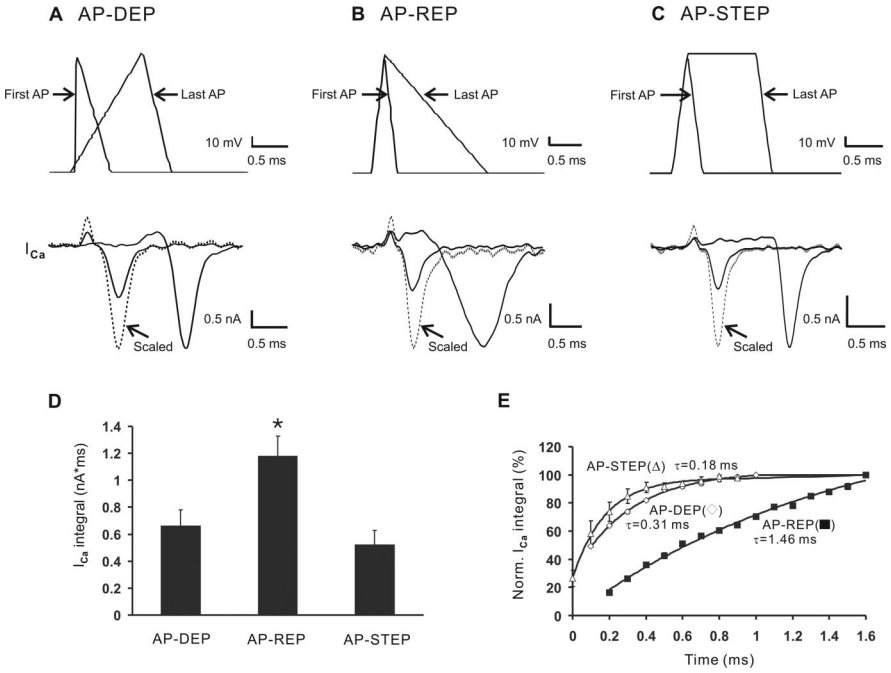

Figure 3. Contribution of the number and kinetics of presynaptic VGCCs to the Ca^{2+} integral during an AP. ***A–C***, I_{Ca} (bottom panels) evoked by the first and the last pseudo-APs (top panels) from each of the three voltage-clamp paradigms in Figure 1. Dotted lines are normalized traces of the first I_{Ca} to the last ones, showing changes in activation and deactivation kinetics. ***D***, The maximal I_{Ca} integrals produced by AP-DEP ($n = 5$), AP-REP ($n = 5$), and AP-STEP ($n = 5$) are plotted. The asterisk indicates that AP-REP causes significantly greater integral of I_{Ca} than AP-DEP and AP-STEP ($p < 0.05$). ***E***, A summary plot of normalized I_{Ca} integrals versus the time of the depolarization (open diamonds), repolarization (filled squares) or plateau phase (open triangles) from these three voltage-ramp protocols. Note that for AP-REP, the integral continues to increase with increasing duration of repolarization and does not appear to saturate. The time constants estimated by fitting the curves with single exponential function are given.

Developmental characteristics of native APs, quantal output, and the fraction of VGCCs recruited by real APs

By systematically changing individual components of pseudo-APs, we have thus far separated the effects of changing the depolarization or repolarization rate on the amplitude and kinetics of I_{Ca} and on quantal output. However, how developmental changes in AP waveform affect synaptic strength remains to be established. To this end, we first characterized the APs evoked by axonal stimulation (axon-APs) from P8–P12 and P16–P18 calyces in both cell-attached voltage-clamp and whole-terminal current-clamp configurations while I_{EPSC} was simultaneously recorded from the postsynaptic neurons (Fig. 5*A*,*B*). In cell-attached configuration, axon-APs were registered as an inward current and an outward current (Fig. 5*A*,*B*, top left panels), the peak of which usually corresponds to the maximal rate of AP depolarization and repolarization, respectively. The peak-to-peak time between these two currents, which approximates the half-width of an AP (Sabatini and Regehr, 1997), was estimated

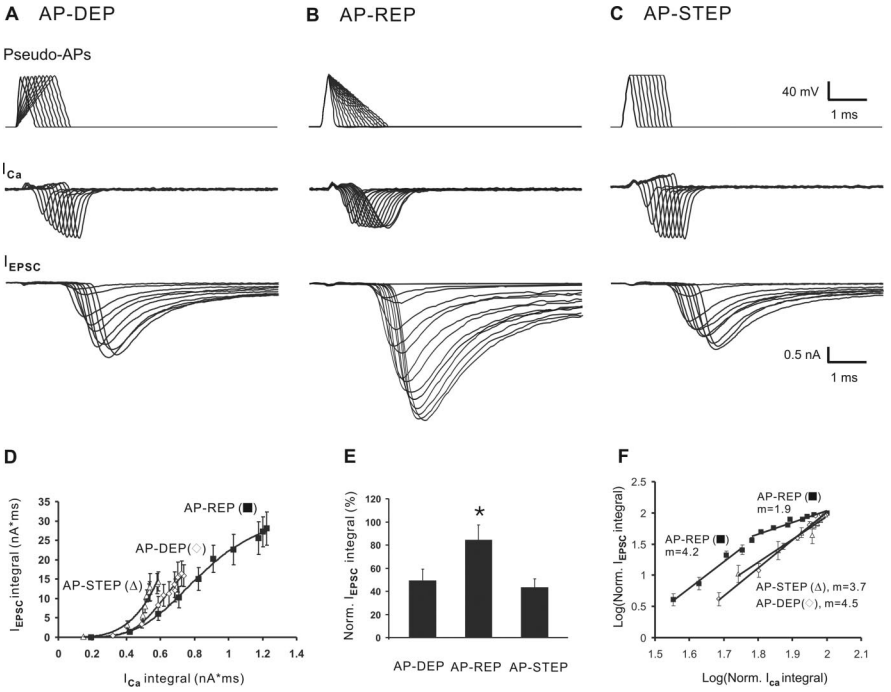

Figure 4. The role of the number and kinetics of VGCCs in controlling transmitter release. ***A–C***, Example recordings of presynaptic I_{Ca} (middle panels) and I_{EPSC} (bottom panels) from the same synapse in response to the voltage ramps (top panels) with increasing depolarization time (***A***, AP-DEP), repolarization time (***B***, AP-REP), or plateau duration (***C***, AP-STEP). ***D***, A plot of the integral of I_{EPSC} versus that of I_{Ca} to show AP-REP (filled squares) generates significantly greater quantal output than AP-DEP (open diamonds) and AP-STEPS (open triangles). ***E***, The maximal I_{EPSC} evoked by each protocol is normalized to the theoretical maximum ($I_{EPSC\text{-}Max}$) obtained by fitting the AP-REP data with the Hill function and plotted to show that both AP-DEP (at 1.0 ms; $n = 5$) and AP-STEP (at 0.9 ms; $n = 5$) produce approximately half of the maximal transmitter release evoked by AP-REP (at 1.6 ms) ($n = 5$). ***F***, The integrals of I_{Ca} and I_{EPSC} normalized to their maximum in each protocol are plotted on a log-log scale. Solid lines are the linear regressions and the cooperativity *m* values are given. Note that the paired data generated by AP-REP are fitted with two linear regressions with two different *m* values.

to be 0.41 ± 0.04 ms ($n = 6$) and 0.26 ± 0.01 ms ($n = 8$, $p < 0.05$) for P8–P12 and P16–P18 synapses, matching well the half-width of APs subsequently recorded from the same calyces (P8–P12: 0.41 ± 0.01 ms; P16–P18: 0.27 ± 0.02; $p < 0.05$) (Fig. 5*C*). In contrast, the amplitude of APs between two age groups was not significantly different, being 109.9 ± 7.3 mV ($n = 6$) and 103.0 ± 4.4 mV ($n = 8$, $p > 0.05$) for P8–P12 and P16–P18 calyces. These observations clearly demonstrated that axon-APs we recorded in current-clamp mode recapitulate developmental AP shortening, attested by the decrease in the peak-to-peak time with noninvasive cell-attached recording configuration that minimally disturbs intraterminal homeostasis. Despite a significant AP shortening, which presumably decreased I_{Ca}, I_{EPSC} recorded in 1 mM $[Ca^{2+}]_e$ before the rupture of presynaptic terminals actually increased in size from 3.36 ± 0.63 nA ($n = 7$) at P8–P12 to 4.72 ± 0.56 ($n = 10$) at P16–P18 (Fig. 5*D*), although not significantly ($p > 0.05$). Such an age-dependent increase in I_{EPSC} is qualitatively consistent with the developmental trend in I_{EPSC} as reported for the mouse calyx of Held synapse in 2 mM $[Ca^{2+}]_e$ (Futai et al., 2001; Joshi and Wang, 2002).

From the above experiments, we selected two axon-APs and used their waveforms as voltage-clamp command templates to measure the fraction of VGCCs recruited by these real APs (Fig. 5*E*, right panel) (AP_I for P8–P12 synapses: amplitude 110 mV with a half-width of 0.4 ms; AP_M for P16–P18 synapses: amplitude 110 mV with a half-width of 0.27 ms). We normalized their amplitude to 110 mV to specifically compare the effects of AP shortening in width on I_{Ca}. In the same calyces, we applied AP_I, AP_M,and a voltage step (10 ms) to evoked I_{Ca}. Because a prolonged step presumably recruits all VGCCs on the calyx, the peak of tail I_{Ca} may be used as the maximal number of channels to estimate the relative fraction of VGCCs activated by real APs. By calculating the amplitude ratio of I_{Ca} evoked by real APs and that by the voltage-step, we found that AP_I and AP_M activated ~50 and 35% of VGCCs (49.7 ± 4.2% vs 34.9 ± 3.8; $p < 0.05$, $n = 4$). Because our previous work showed that the maximal size of I_{Ca} and its voltage dependence are not different between P8–P12 and P16–P18 calyces, but the physical coupling between VGCCs and synaptic vesicles tightens (Fedchyshyn and Wang, 2005), we postulate that developmental AP narrowing is an effective and necessary adaptation for the calyx of Held synapse to reduce the number of VGCCs engaged in triggering transmitter release during an AP.

Development and temperature dependence of quantal output evoked by real APs

To directly examine physiological consequence of AP narrowing, we next compare the effects of AP narrowing on I_{Ca} and I_{EPSC}. Because both depolarization and the repolarization phases speed up concurrently at the developing calyx of Held synapse (Fig. 5) (also see Taschenberger and von Gersdorff, 2000), we designed a series of pseudo-APs (Fig. 6*A*,*B*, top left panels), which had the same amplitude (i.e., −80 to +30 mV, 110 mV) as real APs, but different depolarization and repolarization rates. Using the same synapses, we performed voltage-clamp recordings of presynaptic I_{Ca} evoked by both pseudo-APs and real APs, paired with simultaneous recordings of I_{EPSC} from either the P8–P12 (Fig. 6*A*) or P16–P18 age group (Fig. 6*B*). Independent of the maturity of the synapses, we found that the amplitude of I_{Ca} increased in response to the first few APs and then slightly decreased, as both depolarization and repolarization phases of pseudo-APs were prolonged. The rise and decay time continually increased, leading to a monotonic growth in the total I_{Ca} integral (Fig. 6*C*). In parallel, these kinetic changes in I_{Ca} also led to slower I_{EPSC} rising phase in both age groups (Fig. 6*D*). When the total integrals of I_{Ca} and I_{EPSC} were quantified and plotted against each other (Fig. 6*F*,*G*), both sets of input–output curves were well described by a Hill function. In contrast, the integral or amplitude of I_{EPSC} could not be properly correlated with the amplitude of I_{Ca}, because the I_{Ca} amplitude reached the maximum and then declined, whereas I_{EPSC} continued to increase in response to additional AP broadening (Fig. 6*E*). By fitting input–output curves based on the absolute values of I_{Ca} and I_{EPSC} integrals from P8–P12 ($n = 6$) and P16–P18 synapses ($n = 5$) with the Hill function, we obtained an I_{Ca} integral of 0.70 ± 0.01 nA·ms and 0.48 ± 0.01 nA·ms (I_{EC50}) for the half-maximal quantal output, and the Hill coefficient (n_H) of 3.59 ± 0.14 and 2.85 ± 0.12, respectively (Fig. 6*F*,*G*). This change in n_H parallels the developmental decrease in Ca^{2+}"channel/domain cooperativity" as we previously reported (Fedchyshyn and Wang, 2005), in which we have shown that tighter coupling between

VGCCs and synaptic vesicles in old synapses increases the release efficacy. Indeed, the maximal output ($I_{EPSC\text{-}Max}$) in P16–P18 synapses (38.09 ± 0.64 nA·ms) was significantly higher than that in P8–P12 synapses (25.78 ± 0.44 nA·ms). The increase in the integral of $I_{EPSC\text{-}Max}$ could be somewhat underestimated if translated into the total number of quanta, because developmental subunit switching in AMPARs from slow-gating GluR1-dominant to fast-gating GluR3/4-dominant phenotype (Joshi et al., 2004; Koike-Tani et al., 2005) actually leads to I_{EPSC} with faster kinetics and reduced the integral of unitary quantal event in older synapses.

When real AP templates (i.e., AP_I and AP_M) were used to evoke I_{Ca}, we found that in P8–P12 calyces ($n = 6$), I_{Ca} produced by AP_I and AP_M had a half-width of 0.30 ± 0.02 ms and 0.23 ± 0.01 ms and an average amplitude of 1.21 ± 0.15 nA and 0.79 ± 0.11 nA. In P16–P18 calyces ($n = 5$), I_{Ca} evoked by AP_I and AP_M showed comparable results (half-width: 0.29 ± 0.02 ms and 0.22 ± 0.01 ms; amplitude: 1.38 ± 0.12 nA and 1.14 ± 0.13 nA). Hence, regardless of the maturity of synapses, AP_M generated much faster and smaller I_{Ca} than AP_I, decreasing I_{Ca} integral activated during an AP. The absolute amplitude of I_{EPSC} generated by AP_I was 1.56 ± 0.90 nA for P8–P12 synapses and 4.54 ± 1.40 nA by AP_M for P16–P18 synapses. Compared with that of I_{EPSC} evoked by axonal stimulation for the same age groups (P8–P12: 3.36 ± 0.63 nA; P16–P18: 4.75 ± 0.56 nA) (Fig. 5*D*), the former is substantially lower, and the latter correlates well. The difference in I_{EPSC} generated by axon-APs and by voltage clamp with real APs may be attributed to the difficulty in our selection of real APs (i.e., AP_I) as the voltage-clamp template. Immature calyces exhibit variable AP half-width ranging from 0.3 to 0.6 ms, and small variations in the AP width may lead to big changes in quantal output as a result of high Ca^{2+} cooperativity (m) (Fedchyshyn and Wang, 2005). In contrast, both the AP width and m have stabilized in mature synapses (P16–P18), resulting in a good correlation in I_{EPSC} assayed with two different protocols.

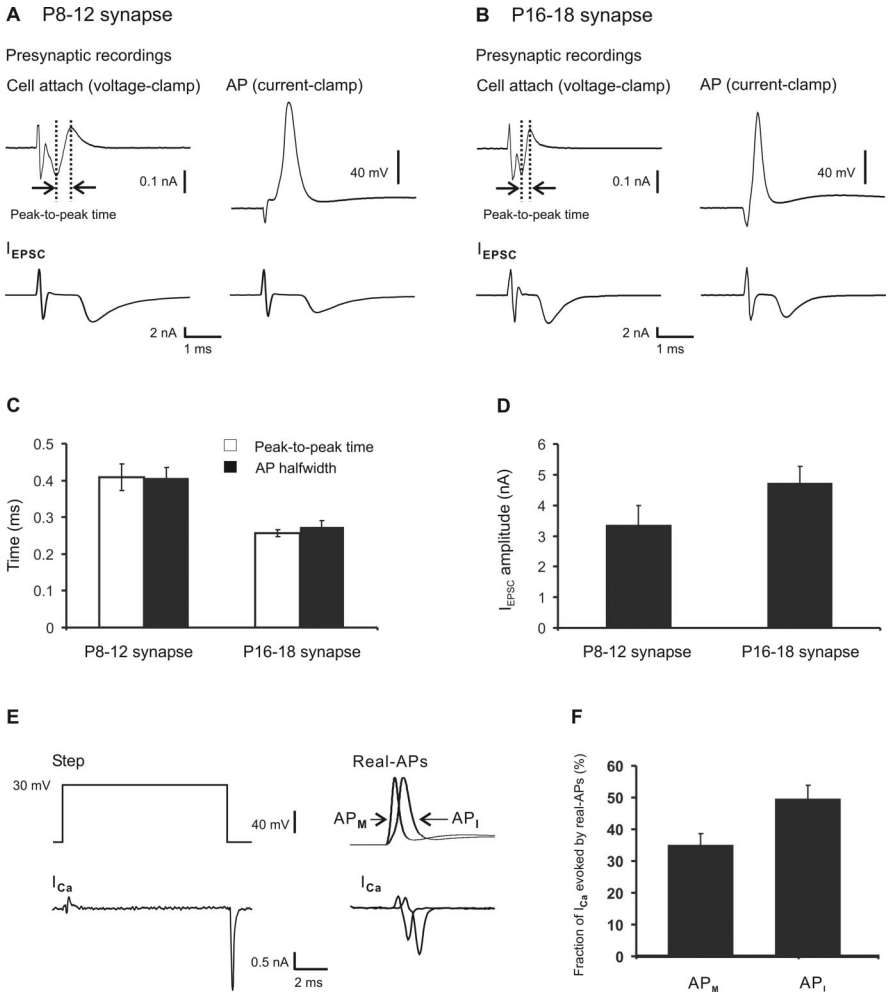

Figure 5. Developmental changes in axon-APs, quantal output, and the fraction of activated VGCCs. ***A***, ***B***, Example recordings of presynaptic responses (top left) in the cell-attached voltage-clamp configuration or APs (top right) in the current-clamp configuration and corresponding I_{EPSC} (bottom panels) generated by stimulation of presynaptic bundle fibers from P8–P12 (***A***) and P16–P18 (***B***) synapses. Dotted lines indicate the relative time between the inward and outward current peaks in cell-attached recordings. ***C***, Comparison of the peak-to-peak time (open bars) and AP half-width (filled bars) recorded from P8–12 ($n = 6$) and P16–P18 synapses ($n = 8$). ***D***, Summary of the amplitude of I_{EPSC} for P8–P12 ($n = 7$) and P16–P18 ($n = 10$) groups. ***E***, Example recordings of presynaptic I_{Ca} (bottom right panel) evoked by real APs (top right panel, AP_I: −80 to 30 mV, depolarization and repolarization time: 0.46 and 0.8 ms, half-width: 0.4 ms; AP_M: −80 to 30 mV, depolarization and repolarization time: 0.2 and 0.5 ms, half-width: 0.27 ms) and that (bottom left panel) produced by a 10 ms voltage step from −70 to 30 mV (top left panel). ***F***, A summary plot of the normalized amplitude of I_{Ca} evoked by real APs to that of the tail current generated by the voltage step.

Cross-correlation analyses of I_{Ca} and I_{EPSC} integrals evoked by real APs with those generated by pseudo-APs showed that AP_M evokes 35.9% less I_{Ca} integral than AP_I (0.25 ± 0.01 nA·ms vs 0.39 ± 0.04 nA·ms) but yields higher I_{EPSC} integrals [3.94 ± 1.04 nA·ms (Fig. 6*G*, blue filled circle)] in P16–P18 synapses than AP_I [2.29 ± 0.32 nA·ms (Fig. 6*F*, red open circle)] in P8–P12 synapses, representing an increase of 72.1% in quantal output. When the two sets of input–output curves are normalized and superimposed (Fig. 6*H*), we noted that AP_I generates ~30% (27.8 ± 0.7%, red open circle) of the total I_{Ca} integral, yielding ~10% of the $I_{EPSC\text{-}Max}$ (9.7 ± 1.4%) for P8–P12 synapses, whereas AP_M produces ~20% (18.0 ± 0.7%, blue filled circle) of the total I_{Ca} integral, resulting in slightly more than 10% of the $I_{EPSC\text{-}Max}$ (11.4 ± 2.9%) for P16–P18 synapses (Fig. 6*H*). Had AP shortening not occurred in P16–P18 synapses, AP_I would generate less than onefold increase in I_{Ca} integral (0.44 ± 0.02 nA·ms) but more than sixfold increase in I_{EPSC} integral (15.98 ± 2.73 nA·ms) (Fig. 6*G*, filled red circle) and fourfold increase in the release fraction per AP (46.5 ± 7.6%) (Fig. 6*H*, filled red circle). These results imply that AP shortening is a necessary adaptation for the calyx to efficiently control quantal output. Despite AP_M generating smaller total I_{Ca} integral than AP_I, a prominent increase in the coupling efficacy counteracts the effects of decreased Ca^{2+} influx produced by narrow AP in mature calyces and effectively maintains the level of quantal output per AP.

It is well known that temperature has a profound impact on AP waveform and transmitter release (Charlton and Atwood, 1979; Sabatini and Regehr; 1996; Kushmerick et al., 2006). To investigate the temperature effect, we recorded APs from P8–P12

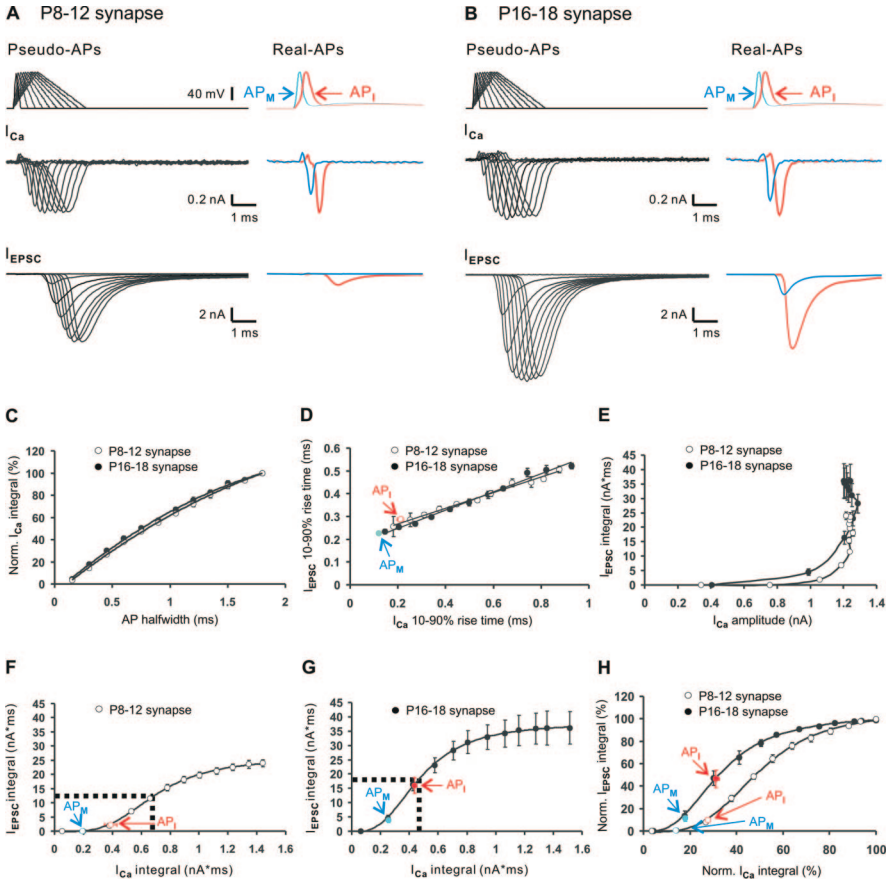

Figure 6. Developmental dependence of quantal output on presynaptic I_{Ca} evoked by real APs. ***A*** and ***B***, Examples of paired recordings of I_{Ca} and I_{EPSC} from P8–P12 (***A***) and P16–P18 (***B***) synapses in response to pseudo-APs (top left panels; −80 to 30 mV; depolarization time from 0.1–1.0 ms with 0.1 ms increments; repolarization time from 0.2 to 2 ms with 0.2 ms increments) and real APs (top right panels, as shown in Figure 5) obtained from P11 and P17 calyces. ***C***, The integrals of I_{Ca} evoked by pseudo-APs recorded from P8–P12 (open circles) and P16–P18 calyces (filled circles) are normalized to the maximal value and plotted against the AP half-width. ***D***, Relationships between the 10–90% rise times of I_{EPSC} and those of I_{Ca} evoked by pseudo-APs and real APs (AP_I: red symbols; AP_M: blue symbols) in P8–P12 (open circles) and P16–P18 synapses (filled circles) are shown. ***E***, A summary plot of the integral of I_{EPSC} versus the amplitude of presynaptic I_{Ca} produced by pseudo-APs at two age groups of synapses. ***F***, ***G***, Plots of the absolute integrals of I_{EPSC} versus that of I_{Ca} recorded from P8–P12 (***F***) and P16–P18 synapses (***G***) in response to pseudo-APs and real APs (AP_I, red symbols; AP_M, blue symbols) showing in ***A*** and ***B***. ***H***, The same plots as in ***F*** and ***G*** except that normalized integrals of I_{EPSC} are plotted against that of I_{Ca} from P8–12 (open circles, $n = 6$) and P16–P18 synapses (filled circles, $n = 5$), respectively. Solid lines in ***F***, ***G***, and ***H*** represent fits with the Hill Function.

calyces ($n = 4$) at the near physiological temperature of 35°C and noted that APs were shortened in width (0.27 ± 0.04 ms) with little change in amplitude (107.3 ± 5.1 mV). We again normalized AP_I at two temperatures to the same amplitude (110 mV) (Fig. 7*A*,*B*, top right panels). Based on these real APs, voltage-command templates were generated for the cross-correlation analyses as in Figure 6. Using immature calyces, we found that both I_{Ca} and I_{EPSC} recorded at 35°C displayed accelerated kinetics, compared with those recorded at 22°C (Fig. 7*A*,*B*). When AP_I was used to evoke I_{Ca}, raising temperature from 22 to 35°C reduced the half-width of I_{Ca} from 0.30 ± 0.02 to 0.22 ± 0.01 ms (Fig. 7*E*) ($p < 0.05$) with little effect on its amplitude (1.21 ± 0.15 and 1.50 ± 0.19 nA). With respect to I_{EPSC} at high temperature, we found that I_{EPSC} saturated at a lower I_{Ca} integral than that at 22°C with a similar maximal quantal output ($I_{EPSC\text{-}Max}$: 25.78 ± 0.44 nA·ms for 22°C vs 26.10 ± 0.45 nA·ms for 35°C) (Fig. 7*C*). Comparison of these two sets of curves indicated that raising temperature led to an upregulation in release efficacy (I_{EC50}: 0.70 ± 0.01 nA·ms for 22°C vs 0.46 ± 0.01 nA·ms for 35°C). AP_I produced similar I_{Ca} integral at 35°C to that at 22°C (0.35 ± 0.03 nA·ms vs 0.39 ± 0.04 nA·ms) but significantly increased I_{EPSC} by 2.9-fold (6.74 ± 2.11 nA·ms vs 2.29 ± 0.32 nA·ms). When the input–output relationship at 35°C was normalized to the maximum and compared with that at 22°C, we again observed a leftward shift in the curve (I_{EC50}: 49.7 ± 0.6% for 22°C vs 41.3 ± 0.5% for 35°C). Although at 35°C AP_I produced a subtle increase in normalized Ca^{2+} integrals (from 27.8 ± 0.7% to 32.0 ± 0.2%), a robust increase in the fraction of I_{EPSC} relative to $I_{EPSC\text{-}Max}$ was observed at a high temperature (AP_I: 9.7 ± 1.4% at 22°C and 27.9 ± 10.6% at 35°C) (Fig. 7*D*). Interestingly, the rise time of I_{EPSC} was also reduced from 0.28 ± 0.01 to 0.23 ± 0.01 ms ($p < 0.05$) when temperature was increased from 22 to 35°C (Fig. 7*F*), implying that fast I_{Ca} transients may help synchronize release events. These results suggest that additional narrowing of APs at 35°C may lead to very brief Ca^{2+} transient but temperature-dependent upregulation in release efficacy downstream from Ca^{2+} influx can boost quantal output by each AP without compromising the synchrony of vesicular release.

Discussion

Integral components of presynaptic I_{Ca} evoked by an AP

In this study, we have taken a reductionist approach to elucidate the effects of different components of an AP on the amplitude and kinetics of presynaptic I_{Ca} and its coupling efficacy for triggering vesicular release. We found that the number of recruited VGCCs, but not their kinetics, is highly sensitive to changes in the AP depolarization phase (Fig. 2*A*). Because the depolarization rate is mainly determined by voltage-gated Na^+ currents, this surprising finding implies that small changes in Na^+ channels, e.g., caused by neuromodulation or neural plasticity (Levitan, 1994; von Gersdorff and Borst, 2002; Engel and Jonas, 2005; Leao et al., 2005), may affect depolarization rate and indirectly modulate the number of active VGCCs during an AP and hence the amount of downstream Ca^{2+} inflow. At the calyx of Held synapse, Na^+ channels ($Na_v1.6$) have been shown to cluster in the axon heminode and upregulate with development, likely underlying the acceleration in the AP depolarization rate or subtle changes in the AP amplitude (Taschenberger and von Gersdorff, 2000; Leao et al., 2005). At this synapse, the density of high-threshold K^+ channels (Kv 3) also shows an age-dependent increase, which may contribute to the rapid repolarization phase (Dodson et al., 2003; Elezgarai et al., 2003; Ishikawa et al., 2003). Our experiments with AP-REP paradigm demonstrated that the repolarization phase is also involved in determining the number of activated VGCCs, particularly when the AP width is narrow, as manifested by the increase in the I_{Ca} amplitude with AP broadening. However, the kinetic component of activated VGCCs becomes the dominant contributor to the total Ca^{2+} integral once the I_{Ca} amplitude saturates (Fig. 2*B*,*D*).

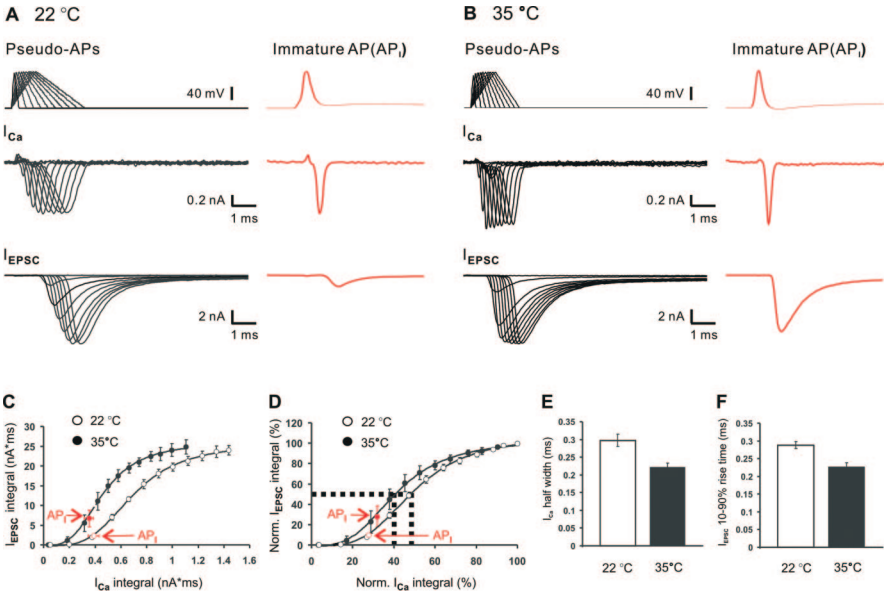

Figure 7. The effects of temperature on I_{Ca} and transmitter release. ***A***, ***B***, Examples of paired recordings of I_{Ca} and I_{EPSC} produced by pseudo-APs (left panels) and real APs (right panels) at 22°C (***A***) and 35°C (***B***) from P8–P12 synapses are shown. Note the difference in pseudo-APs and real APs between the two temperature conditions (***B***). In ***B***, real AP (top right panel) was recorded at 35°C from a P11 calyx (AP_I, red lines, −80 to 30 mV; depolarization and repolarization time, 0.4 and 0.5 ms; half-width, 0.3 ms). Pseudo-APs with fast kinetics (top left panel; −80 to 30 mV, depolarization and repolarization time, from 0.1 to 1.0 ms with 0.1 ms increments) were designed accordingly. ***C***, The integrals of I_{EPSC} recorded at 22°C (open circles, $n = 6$) and 35°C (filled circles, $n = 4$) are plotted against the total integrals of I_{Ca} evoked by pseudo-APs and immature APs. ***D***, The same plots as in ***C*** except that normalized integrals of I_{Ca} and I_{EPSC} are presented and solid lines are the fitting curves with the Hill function. ***E***, ***F***, Summary plots of the half-width of I_{Ca} (***E***) and the rise time of I_{EPSC} (***F***) produced by real immature APs at 22°C (open bars, $n = 6$) and 35°C (filled bars, $n = 4$).

Our observations may help reconcile the opposing views on the effect of spike broadening on presynaptic I_{Ca} among different synapses. At the squid giant synapse, classical work showed that an AP opens only a small fraction of presynaptic VGCCs (~10%) (Pumplin et al., 1981; Llinas et al., 1982) and that AP broadening enhances calcium entry primarily by increasing the number of calcium channels that open, leading to large increases in the amplitude of I_{Ca} (Augustine, 1990). In contrast, theoretical computer simulations and experimental evidence in central synapses, including the calyx of Held synapse, demonstrate that an AP effectively opens a majority of VGCCs (>70%), and AP broadening increases calcium influx mainly, if not exclusively, by prolonging the kinetics of calcium currents with little effect on the amplitude of I_{Ca} (Sabatini and Regehr, 1997; Borst and Sakmann, 1998, 1999; Geiger and Jonas, 2000; Bischofberger et al., 2002). In fact, much of the past work done in central synapses was based on biophysical properties of VGCCs in immature terminals, in which propagating APs usually have wide waveform [e.g., cerebellar granule–Purkinje cell synapse with AP half-width ~1 ms from P10–P18 rats (Sabatini and Regehr, 1997); hippocampal mossy fiber–CA3 synapse with AP half-width ~0.85 ms from P20–28 rats (Geiger and Jonas, 2000; Bischofberger et al., 2002); calyx of Held synapse with AP half-width ~0.5 ms from P8–P10 rats (Borst and Sakmann 1998, 1999)]. As a result, AP broadening will only reveal changes in the I_{Ca} kinetics but not its amplitude. It is, however, conceivable that the differences in the AP amplitude among various synapses may also contribute to the apparent discrepancy. In addition, experiments in invertebrate synapses were usually performed at lower temperatures (e.g., 18°C for squid giant synapse) than those in central synapses, which may significantly slow the activation and deactivation kinetics of VGCCs and reduce the fraction of VGCCs recruited by an AP.

In this study, we have recapitulated distinct aspects of the AP broadening effects described in different synapses. In the experiments with real APs (Fig. 5), AP_I (half-width, 0.4 ms) and AP_M (half-width, 0.27 ms) elicited ~50 and 35% of the maximal I_{Ca}. The former value is lower than that (~70%) reported for the rat immature calyx in Borst and Sakmann (1998), but this may be accounted for by the difference in the AP width (i.e., 0.4 vs 0.5 ms) and other subtle difference in experimental protocols. Regardless of the developmental stage of this synapse, AP_M always activates a smaller fraction of VGCCs than AP_I, leaving the remaining channels for additional recruitment by AP broadening before the kinetic changes of I_{Ca} become the predominant contributor to the total integral (Figs. 6, 7). Therefore, the initial AP width defined by depolarization and repolarization time course may dictate whether AP broadening induces changes in the amplitude or the kinetics of I_{Ca}. We suggest that by accelerating AP depolarization and repolarization rates, developmental AP shortening at the calyx of Held synapse primarily reduces the number of VGCCs recruited by an AP and ensures the brevity of Ca^{2+} transients.

Efficacy of presynaptic I_{Ca} in triggering transmitter release

We have used paired recordings to characterize the coupling efficacy of presynaptic I_{Ca} evoked by various pseudo- and real APs with transmitter release. Probing with AP-DEP, AP-REP, and AP-STEP, we found that both the number of VGCCs and their kinetics contributed to the total Ca^{2+} integral (Fig. 3), with each of the two components contributing to ~50% of the maximal quantal output (Fig. 4). Experiments with other pseudo-AP paradigms (Figs. 6, 7), mimicking concurrent changes in both depolarization and repolarization phases during development, demonstrate that there is a strong dependence of quantal output on the total integral of I_{Ca}, with all input–output relationships being well described by the Hill function independent of synaptic maturity and temperature (correlation coefficient $R > 0.95$ in all cases). By manipulating both the number and kinetic components of activated VGCCs, synapses may effectively expand their dynamic operating range and potentially present disparate targets for neuromodulation.

Our observations are in line with the notion that the integral of the Ca^{2+} transient rather than its amplitude determines the efficacy of transmitter release (Bollmann and Sakmann, 2005). AP narrowing from AP_M to AP_I decreases absolute I_{Ca} integral by ~36% while I_{EPSC} increases by 72%, indicating enhanced synaptic strength. Cross-correlation analyses of normalized input–output curves between pseudo-APs and real APs revealed that AP_I in P8–P12 synapses generates ~28% of the maximal I_{Ca} integral and sets I_{EPSC} <10% of the $I_{EPSC\text{-}Max}$, whereas AP_M in P16–P18 synapses significantly decreased the total I_{Ca} integral to ~18% and yet maintained I_{EPSC} at 11% of the $I_{EPSC\text{-}Max}$ (Fig. 6).

The mechanism underlying such a stability in the release fraction evoked by a reduced Ca^{2+} integral may reside in the opposing action of enhanced coupling efficacy, as evidenced by an age-dependent leftward shift in the input–output curve and an increase in $I_{EPSC\text{-}Max}$. We have demonstrated previously that the spatial coupling between VGCCs and synaptic vesicles tightens as maturation progresses, transforming the release modality from loosely coupled "microdomain" to tightly coupled "nanodomain" (Fedchyshyn and Wang, 2005). Such a transformation in the active zones evidently enhances the coupling efficacy of Ca^{2+} influx to vesicular fusion. Similarly, raising temperature in immature synapses can also increase the coupling efficacy by reducing the minimal number of overlapping domains required for triggering release of single vesicles (Fedchyshyn and Wang, 2005). Hence, the effect of AP shortening on I_{Ca} can be counteracted by the increase in coupling efficacy. An additional extrapolation from our results is that the calyx of Held synapse at maturity has built up the mechanisms for controlling quantal output by regulating the number of recruited VGCCs and their couplings to synaptic vesicles, releasing transmitters in a manner reminiscent of that at the squid giant synapse (Llinas et al., 1981, 1982; Pumplin et al., 1981; Augustine, 1990).

Physiological implications of developmental AP shortening in high-fidelity and high-frequency synaptic transmission

At any central synapse, the relationship between the amount of Ca^{2+} influx and quantal output can be approximated by a power function in the form of $I_{EPSC} \alpha [I_{Ca}]^m$, where m denotes Ca^{2+} cooperativity (Dodge and Rahamimoff, 1967). Experiments presented in this study demonstrate that AP narrowing is a highly effective adaptation for the calyx to reduce I_{Ca} integral. We have demonstrated that both developmental maturation and high temperature reduce the m value (Fedchyshyn and Wang, 2005). In the context of these lines of evidence, we suggest that the developmental reductions in I_{Ca} and m converge to constrain the number of synaptic vesicles released, whereas parallel upregulation of both coupling efficacy downstream from Ca^{2+} entry and the number of active zones at the mature calyx (~600) (Taschenberger et al., 2002) may counteract such effects. Ultimately, synaptic strength is enhanced while the release fraction per AP is maintained. These adaptations help prevent the terminal from depleting the readily releasable pool of synaptic vesicles during high-frequency synaptic activity (Wang and Kaczmarek, 1998; Schneggenburger et al., 1999; Iwasaki and Takahashi, 2001; Taschenberger et al., 2002). Furthermore, small and brief I_{Ca} generated by narrow APs promotes synchronized release events (Fig. 7*F*) and hence the fidelity of synaptic transmission. Such biophysical plasticity along with concurrent morphological reorganization in active zones (von Gersdorff and Borst, 2002) is likely important for the development of high-fidelity neurotransmission required for sound localization at this synapse.

References

Augustine G (1990) Regulation of transmitter release at the squid giant synapse by presynaptic delayed rectifier potassium current. J Physiol (Lond) 431:343–364.

Bischofberger J, Geiger JR, Jonas P (2002) Timing and efficacy of Ca^{2+} channel activation in hippocampal mossy fiber boutons. J Neurosci 22:10593–10602.

Bollmann JH, Sakmann B (2005) Control of synaptic strength and timing by the release-site Ca^{2+} signal. Nat Neurosci 8:426–434.

Borst JG, Sakmann B (1998) Calcium current during a single action potential in a large presynaptic terminal of the rat brainstem. J Physiol (Lond) 506:143–157.

Borst JG, Sakmann B (1999) Effect of changes in action potential shape on calcium currents and transmitter release in a calyx-type synapse of the rat auditory brainstem. Philos Trans R Soc Lond B Biol Sci 354:347–355.

Borst JG, Helmchen F, Sakmann B (1995) Pre- and postsynaptic whole-cell recordings in the medial nucleus of the trapezoid body of the rat. J Physiol (Lond) 489:825–840.

Borst JGG, Sakmann B (1996) Calcium influx and transmitter release in a fast CNS synapse. Nature 383:431–434.

Charlton MP, Atwood HL (1979) Synaptic transmission: temperature-sensitivity of calcium entry in presynaptic terminals. Brain Res 170:543–546.

Colecraft HM, Patil PG, Yue DT (2000) Differential occurrence of reluctant openings in G-protein-inhibited N- and P/Q-type calcium channels. J Gen Physiol 115:175–192.

Delaney K, Tank DW, Zucker RS (1991) Presynaptic calcium- and serotonin-mediated enhancement of transmitter release at crayfish neuromuscular junction. J Neurosci 11:2631–2643.

Dodge FA, Rahamimoff R (1967) Co-operative action of calcium ions in transmitter release at the neuromuscular junction. J Physiol (Lond) 193:419–432.

Dodson PD, Billups B, Rusznak Z, Szucs G, Barker MC, Forsythe ID (2003) Presynaptic rat Kv1.2 channels suppress synaptic terminal hyperexcitability following action potential invasion. J Physiol (Lond) 550:27–33.

Elezgarai I, Diez J, Puente N, Azkue JJ, Benitez R, Bilbao A, Knopfel T, Donate-Oliver F, Grandes P (2003) Subcellular localization of the voltage-dependent potassium channel Kv3.1b in postnatal and adult rat medial nucleus of the trapezoid body. Neuroscience 118:889–898.

Engel D, Jonas P (2005) Presynaptic action potential amplification by voltage-gated Na+ channels in hippocampal mossy fiber boutons. Neuron 45:405–417.

Fedchyshyn MJ, Wang LY (2005) Developmental transformation of the release modality at the calyx of held synapse. J Neurosci 25:4131–4140.

Forsythe ID (1994) Direct patch recording from identified presynaptic terminals mediating glutamatergic EPSCs in the rat CNS, in vitro. J Physiol (Lond) 479:381–387.

Forsythe ID, Barnes-Davies M (1993) The binaural auditory pathway: excitatory amino acid receptors mediate dual time course excitatory postsynaptic currents in the rat medial nucleus of the trapezoid body. Proc R Soc Lond B Biol Sci 251:151–157.

Futai K, Okada M, Matsuyama K, Takahashi T (2001) High-fidelity transmission acquired via a developmental decrease in NMDA receptor expression at an auditory synapse. J Neurosci 21:3342–3349.

Geiger JR, Jonas P (2000) Dynamic control of presynaptic Ca(2+) inflow by fast-inactivating K(+) channels in hippocampal mossy fiber boutons. Neuron 28:927–939.

Gentile L, Stanley EF (2004) A unified model of presynaptic release site gating by calcium channel domains. Eur J Neurosci 21:278–282.

Ishikawa T, Nakamura Y, Saitoh N, Li WB, Iwasaki S, Takahashi T (2003) Distinct roles of Kv1 and Kv3 potassium channels at the calyx of Held presynaptic terminal. J Neurosci 23:10445–10453.

Iwasaki S, Takahashi T (2001) Developmental regulation of transmitter release at the calyx of Held in rat auditory brainstem. J Physiol (Lond) 534:861–871.

Joshi I, Wang LY (2002) Developmental profiles of glutamate receptors and synaptic transmission at a single synapse in the mouse auditory brainstem. J Physiol (Lond) 540:861–873.

Joshi I, Shokralla S, Titis P, Wang LY (2004) The role of AMPA receptor gating in the development of high-fidelity neurotransmission at the calyx of Held synapse. J Neurosci 24:183–196.

Klein M, Kandel ER (1980) Mechanism of calcium current modualtion underlying presynaptic facilitation and behavioral sensitization in *Aplysia.* Proc Natl Acad Sci USA 77:6912–6916.

Koike-Tani M, Saitoh N, Takahashi T (2005) Mechanisms underlying developmental speeding in AMPA-EPSC decay time at the calyx of Held. J Neurosci 25:199–207.

Kushmerick C, Renden R, von Gersdorff H (2006) Physiological temperatures reduce the rate of vesicle pool depletion and short-term depression via an acceleration of vesicle recruitment. J Neurosci 26:1366–1377.

Leao RM, Kushmerick C, Pinaud R, Renden R, Li GL, Taschenberger H, Spirou G, Levinson SR, von Gersdorff H (2005) Presynaptic Na+ channels: locus, development, and recovery from inactivation at a high-fidelity synapse. J Neurosci 25:3724–3738.

Levitan IB (1994) Modulation of ion channels by protein phosphorylation and dephosphorylation. Annu Rev Physiol 56:193–212.

Llinas R, Steinberg IZ, Walton K (1981) Relationship between presynaptic calcium current and postsynaptic potential in squid giant synapse. Biophys J 33:323–352.

Llinas R, Sugimori M, Simon SM (1982) Transmission by presynaptic spike-like depolarization in the squid giant synapse. Proc Natl Acad Sci USA 79:2415–2419.

Mintz IM, Sabatini BL, Regehr WG (1995) Calcium control of transmitter release at a cerebellar synapse. Neuron 15:675–688.

Pumplin DW, Reese TS, Llinas R (1981) Are the presynaptic membrane particles the calcium channels? Proc Natl Acad Sci USA 78:7210–7213.

Sabatini BL, Regehr WG (1996) Timing of neurotransmission at fast synapses in the mammalian brain. Nature 384:170–172.

Sabatini BL, Regehr WG (1997) Control of neurotransmitter release by presynaptic waveform at the granule cell to Purkinje cell synapse. J Neurosci 17:3425–3435.

Schneggenburger R, Meyer AC, Neher E (1999) Released fraction and total size of a pool of immediately available transmitter quanta at a calyx synapse. Neuron 23:399–409.

Taschenberger H, von Gersdorff H (2000) Fine-tuning an auditory synapse for speed and fidelity: developmental changes in presynaptic waveform, EPSC kinetics, and synaptic plasticity. J Neurosci 20:9162–9173.

Taschenberger H, Leao RM, Rowland KC, Spirou GA, von Gersdorff H (2002) Optimizing synaptic architecture and efficiency for high-frequency transmission. Neuron 36:1127–1143.

Trussell LO (1999) Synaptic mechanisms for coding timing in auditory neurons. Annu Rev Physiol 61:477–496.

von Gersdorff H, Borst JG (2002) Short-term plasticity at the calyx of Held. Nat Rev Neurosci 3:53–64.

Wang LY, Kaczmarek LK (1998) High-frequency firing helps replenish the readily releasable pool of synaptic vesicles. Nature 394:384–388.

Wu LG, Saggau P (1994) Pharmacological identification of two types of presynaptic voltage-dependent calcium channels at CA3–CA1 synapses of the hippocampus. J Neurosci 14:5613–5622.

Wu LG, Westenbroek RE, Borst JG, Catterall WA, Sakmann B (1999) Calcium channel types with distinct presynaptic localization couple differentially to transmitter release in single calyx-type synapses. J Neurosci 19:726–736.

Wu XS, Sun JY, Evers AS, Crowder M, Wu LG (2004) Isoflurane inhibits transmitter release and the presynaptic action potential. Anesthesiology 100:663–670.